INVITED PAPER   *Special Section on Fundamentals and Applications of Advanced Semiconductor Devices*

Beating Analysis of Shubnikov de Haas Oscillation in In$_{0.53}$Ga$_{0.47}$As Double Quantum Well toward Spin Filter Applications

Takaaki KOGA[†a]**, Toru MATSUURA**[††]**, Sébastien FANIEL**[†††]**,** *Nonmembers,* **Satofumi SOUMA**[††††]**,** *Member,*
Shunsuke MINESHIGE[†]**, Yoshiaki SEKINE**[†††††]**,** *and* **Hiroki SUGIYAMA**[††††††]**,** *Nonmembers*

SUMMARY   We recently determined the values of intrinsic spin-orbit (SO) parameters for In$_{0.52}$Al$_{0.48}$As/In$_{0.53}$Ga$_{0.47}$As(10 nm)/In$_{0.52}$Al$_{0.48}$As (InGaAs/InAlAs) quantum wells (QW), lattice-matched to (001) InP, from the weak localization/antilocalization analysis of the low-temperature magneto-conductivity measurements [1]. We have then studied the sub-band energy spectra for the InGaAs/InAlAs double QW system from beatings in the Shubnikov de Haas (SdH) oscillations. The basic properties obtained here for the double QW system provides useful information for realizing nonmagnetic spin-filter devices based on the spin-orbit interaction [2].
key words: quantum well, spin-orbit interaction, Shubnikov de Haas oscillation, Rashba effect, spin filter

1. Introduction

InGaAs/InAlAs quantum wells (QW) are considered as promising base materials for spintronics applications that utilize the spin-orbit interaction [1], [2]. Main reasons for this include (1) InGaAs/InAlAs QWs are a lattice-matched system to (001) InP substrate, providing a high-quality, strain-free host for the conduction electrons, and (2) zero-field spin splitting (ZFSS) based on the structural inversion asymmetry (SIA), so-called the Rashba effect [3], is relatively large in this system, comparing to the GaAs/AlGaAs QWs, for example, whose magnitude is gate-controllable [4], [5]. We also recently discovered that the ZFSS based on the bulk inversion asymmetry (BIA), so-called the Dresselhaus effect [6], is mostly negligible relative to the Rashba effect in this system [1].

In this paper, we first present weak localization/antilocalization data for an InGaAs/InAlAs single QW, from which the values of the spin-orbit (SO) coefficients were de-

termined quantitatively (Sect. 2). The values of SO coefficients provide essential information for designing a non-magnetic spin-filter device using the double QW system (Sect. 3). We, then, present electron transport properties of the double QWs, composed of the InGaAs/InAlAs epitaxial heterostructures, at low temperatures (1.4 K) in Sect. 4. In Sect. 5, discussions were made on the experimental data provided in Sect. 4, including the comparison with the theoretical simulation results. In the present work, we rather focused on the subband energy splitting in the double QW system and leave the arguments on the spin splitting in double QW system for the future work.

2. Basic Properties of Single Quantum Well

2.1 Spin-Orbit Coefficients Determined by the Weak Localization/Antilocalization Analysis

Recently, we reported the determination of the intrinsic parameters for the SO interaction in In$_{0.53}$Ga$_{0.47}$As/In$_{0.52}$-Al$_{0.48}$As single QWs from the analysis of the weak antilocalization (WAL) measurements [1]. We find that the Dresselhaus SO [6] is mostly negligible in this system and that the intrinsic parameter for the Rashba effect, a$_{SO} \equiv \alpha/\langle E_z \rangle$, is determined quantitatively to be a$_{SO}m^*/m_e = (1.46 - 1.51 \times 10^{-17}N_S \text{ [m}^{-2}]) \, e\text{Å}^2$, where α is the Rashba coefficient, $\langle E_z \rangle$ is the expected electric field within the QW normal to the plane, m^*/m_e is the electron effective mass ratio, and N_S is the sheet carrier density. These values for a$_{SO}m^*$ were also confirmed by the observation of beatings in the Shubnikov — de Haas (SdH) oscillations in our most asymmetric QW sample [1].

The weak localization/antilocalization measurements of In$_{0.52}$Al$_{0.48}$As/In$_{0.53}$Ga$_{0.47}$As(10 nm)/In$_{0.52}$Al$_{0.48}$As QWs were performed using Hall bar samples of the size 125 μm × 250 μm at dilution temperatures [1], [5]. In Fig. 1, we show the magneto-conductance data for sample KH1-3 at dilution temperature (T_{base}=20 mK), where we clearly see that the WAL effect is minimized near the carrier density $N_S^* \equiv 1.06 \times 10^{16} \text{ m}^{-2}$. We can conclude that the Rashba coefficient α is minimized at N_S^*, where $\langle E_z \rangle = 0$ is realized.

Figure 2 shows the plot of $\tilde{\alpha}m^*/m_e$, a phenomenological measure for the strength of the SO interaction, as a function of N_S. Note that $\tilde{\alpha}m^*$ is defined as $(e\hbar^3 B_{\text{min}})^{1/2}$ [1], letting B_{min} be the marked magnetic field in Fig. 1, where the magneto-conductivity is at the local minimum. We see

Fig. 1 Weak antilocalization data obtained for an InGaAs/InAlAs single QW (sample KH1-3). Measurements were performed using a 125 μm × 250 μm Hall bar, fabricated by photolithography, at dilution temperatures ($T_{base} \approx 20$ mK at the sample holder Cu block). The magnetic fields B were applied perpendicular to the QW plane. Each trace, shifted vertically for better presentation, is for different N_S that is controlled by gate. The vertical marks in each trace indicate the places of B_{min}. Solid curves for N_S = 0.78, 0.84, 1.27 and 1.33 × 10^{16} m^{-2} are theoretical fits to the experimental data using the Golub model [7].
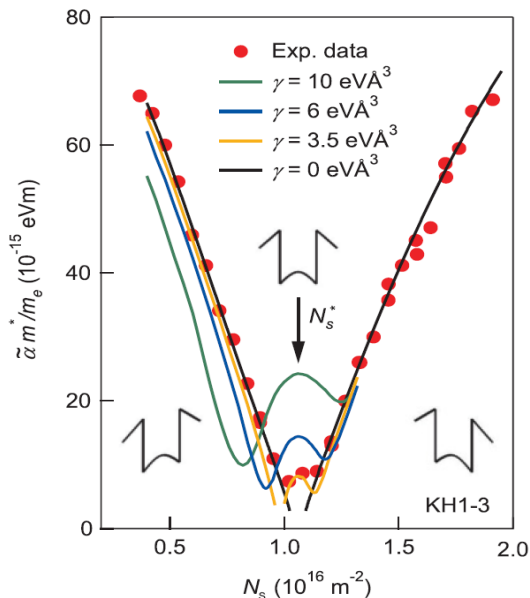
Fig. 2 Strength of the SO interaction (ordinate) as a function of N_S. Closed circles are the experimental data. Curves are the simulated results assuming various values for the Dresselhaus parameter γ, showing that the experimental data contradict the assumption $\gamma > 3.5$ eVÅ^3 [1]. Also shown in the figure are the sketches of the corresponding QW potential shapes and the position of N_S^* where the QW potential is supposed to retain a symmetric shape.
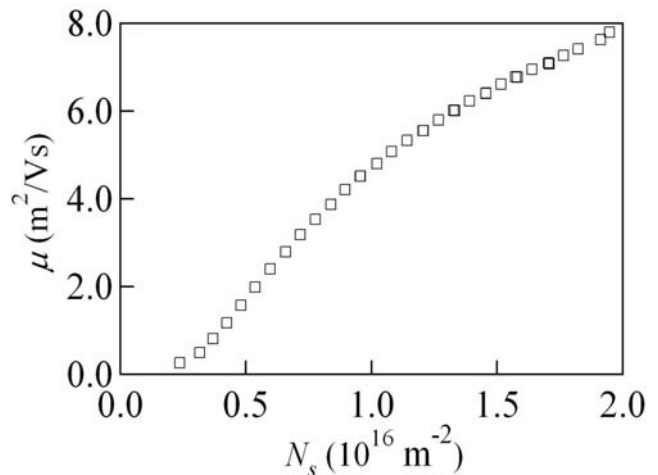
Fig. 3 Electron mobility μ of sample KH1-3 at dilution temperature ($T_{base} = 20$ mK) as a function of the gate-controlled N_S.

that $\tilde{\alpha}m^*/m_e$ is minimized at N_S^*, as expected, and increases almost linearly with $|N_S - N_S^*|$, since $|N_S - N_S^*|$ is proportional to $\langle E_z \rangle$ according to the the Poisson equation. This observation is consistent with the Rashba mechanism $\alpha \propto \langle E_z \rangle$.

2.2 Electron Mobility of Single Quantum Well

Plotted in Fig. 3 are the electron mobility μ deduced from the measured longitudinal resistivity ρ_{xx} ($\mu \equiv 1/eN_S\rho_{xx}$, e being electron's charge) of sample KH1-3 at dilution temperature ($T_{base} = 20$ mK), as a function of the gate-controlled N_S. The extraction of N_S values was made from the Shubnikov-de Haas and Hall measurements. The N_S values deduced from these measurements agreed within an accuracy of a few percent. It is noted that μ values at 1.4 K are essentially same as those at T_{base}=20 mK, hence providing useful information for the analysis of the double QW system discussed in Sects. 3–5.

3. Design of Double Quantum Well System

3.1 Layer Structure

Shown in Fig. 4 is the schematic layer structure of the double QW sample used in the present experiment. These samples were grown by the Metal-Organic Chemical Vapor Deposition (MOCVD) on a semi-insulating (001) InP substrate epitaxially. The active part of the layers is the pair of 10 nm-thick QWs made of non-doped (but, remotely doped to be n-type) In$_{0.53}$Ga$_{0.47}$As, where these two QWs are separated by a barrier layer made of In$_{0.52}$Al$_{0.48}$As whose thickness d_B ranges from 1.5 nm to 5 nm. 6 nm-thick n-doped (Si) carrier supplying layers are placed both above and below the QW layers, separated with 6 nm-thick non-doped spacers. The doping densities in the carrier supplying layers, denoted as n_1 and n_2 in Fig. 4, are typically 2×10^{18} cm^{-3}. We call the QW located in the substrate side QW1 and that located in the surface side QW2.

| i-In$_{0.52}$Al$_{0.48}$As (5 nm) |
| i-AlAs (1.5 nm) |
| i-In$_{0.52}$Al$_{0.48}$As (d_{sk}=25 nm) |
| n-In$_{0.52}$Al$_{0.48}$As (6 nm) n_2 |
| i-In$_{0.52}$Al$_{0.48}$As (6 nm) |
| i-In$_{0.53}$Ga$_{0.47}$As (d_{OW} nm) QW2 |
| i-In$_{0.52}$Al$_{0.48}$As (d_B nm) |
| i-In$_{0.53}$Ga$_{0.47}$As (d_{OW} nm) QW1 |
| i-In$_{0.52}$Al$_{0.48}$As (6 nm) |
| n-In$_{0.52}$Al$_{0.48}$As (6 nm) n_1 |
| i-In$_{0.52}$Al$_{0.48}$As (200 nm) |
| (001) InP Substrate |

Fig. 4 Schematic layer structure for the double QW sample used in the present experiment.

3.2 Device Structure and Measurement

Gated Hall bar devices of the size $125 \mu m \times 250 \mu m$ were fabricated by photolithography using 30 nm thick HfO$_2$ as a gate insulator that was grown by the atomic layer deposition. The electron transport measurements were performed using a standard lock-in technique in a ^{4}He cryostat (base temperature 1.4 K). The exciting current used in the measurement was typically 100 nA whose frequencies were 11–183 Hz. External magnetic fields were applied perpendicularly to the QW layers using a superconducting solenoid.

4. Experimental Results

Shown in Fig. 5 is the plot of relative electric resistance R_{xx} as a function of magnetic field for a d_B=3 nm sample, exhibiting the Shubnikov-de Haas (SdH) oscillations, at various gate voltages. We find that each oscillation consists of two frequencies, which results in beatings in the oscillations. The positions of the beating nodes are indicated by the vertical arrows in Fig. 5. A physical origin for these beatings is the co-existence of different types of carriers, occupying different subbands, for example, whose sheet carrier densities slightly differ from each other. Such situation can be caused either by the subband splitting in the double QW system or by spin splitting due to the Rashba effect. Indeed, we are interested in the transition (or interplay) between the subband and Rashba splittings [8].

In our measurements, we indeed observed two distinct types of beatings in the SdH oscillations. One is attributed to the spin splitting ($B < 2$ T, not shown here) and the other to the subband splitting ($B > 2$ T, nodes indicated by the arrows in Fig. 5). In the present paper, we show our analysis on the subband splitting only, since it is more fundamental issue than the spin splitting. We leave the discussions on the
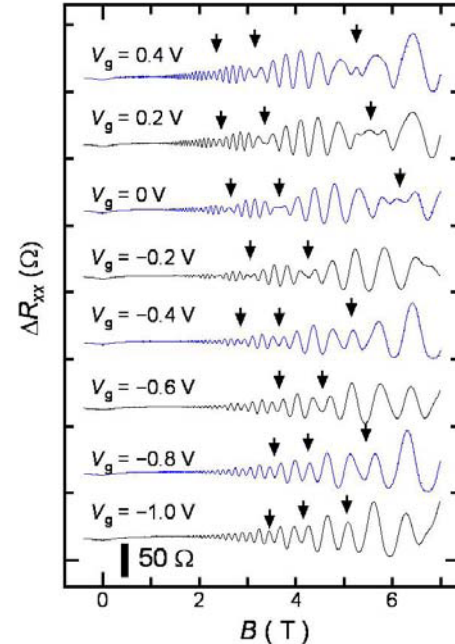

Fig. 5 Shubnikov-de Haas oscillations for $d_B = 3$ nm sample with various gate voltages. The temperature for the measurements is 1.4 K. The positions of the observed beating nodes are marked by the vertical arrows. The traces are shifted vertically for better presentation.

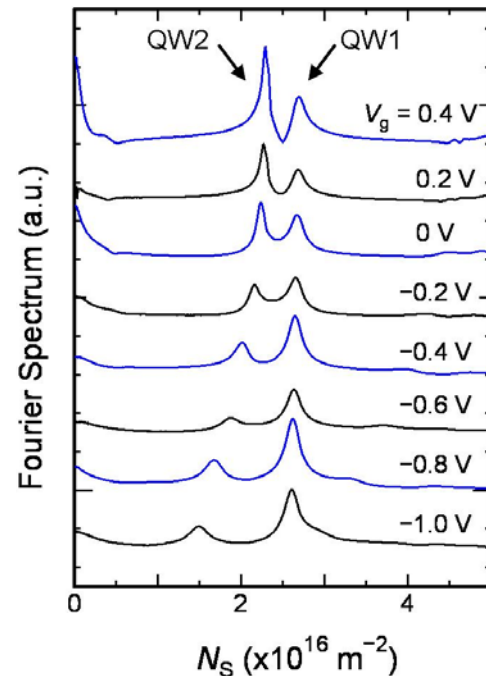**Fig. 6** Amplitude of Fourier transform spectrum for the data plotted in Fig. 5 after re-plotting the data as a function of $1/B$. The abscissa in this figure is converted to the sheet carrier density N_S.

SdH beating originating from the Rashba splitting for the future work.

To extract quantitative values of the sheet carrier densities for each subband, denoted as N_{S1} and N_{S2}, from the SdH
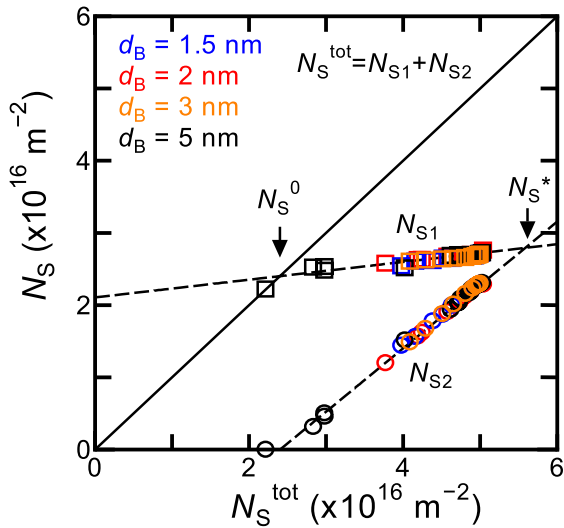
Fig. 7 Plot of the electron sheet carrier densities N_{S1} and N_{S2} that are assigned for QW1 and QW2, respectively. The data are plotted as a function of the total sheet carrier density $N_S^{tot} = N_{S1} + N_{S2}$.

measurements, we performed the Fourier transform (FT) on the measured data in Fig. 5 after converting the abscissa to $1/B$ and subtracting the slowly varying background that is pronounced in the small magnetic field regime ($B < 1$ T) using polynomial fits (see Fig. 5). In Fig. 6, we find two peaks in each trace of FT spectrum curves, corresponding to the occupation of multiple subbands in the double QW system. We note that the peak at the higher density (N_{S1}) originates from QW1, whereas the peak at the lower density (N_{S2}) does from QW2 as we discuss below.

Figure 7 shows the plot of the electron sheet carrier densities originating from QW1 and QW2, denoted as N_{S1} and N_{S2}, respectively, as a function of the total sheet carrier density $N_S^{tot} = N_{S1} + N_{S2}$. We define N_S^0 as the sheet carrier density below which only the lowest subband is occupied with electrons [see Fig. 8(a)]. We also define N_S^* as the sheet carrier density where the QW potential retains the symmetrical shape about the middle barrier layer, allowing the formation of the bonding and anti-bonding wave functions, denoted as Ψ_1 (the lowest subbnad) and Ψ_2 (the second lowest subband), respectively [see Fig. 8(c)].

5. Theoretical Simulation of SdH Oscillations

5.1 Simulation Method

In Fig. 6, we find that the heights of the two peaks in the FT spectrum are always different from each other. Particularly, the peak originating from QW2 is lower than that from QW1 for $V_g \leq -0.2$ V, whereas the peak originating from QW1 is lower than that from QW2 for $V_g \geq 0$ V. To better understand the transport properties of the double QWs including the physical mechanism of the above features in the FT spectrum of SdH oscillations, we performed theoretical simulations of the SdH oscillations for the double QWs,
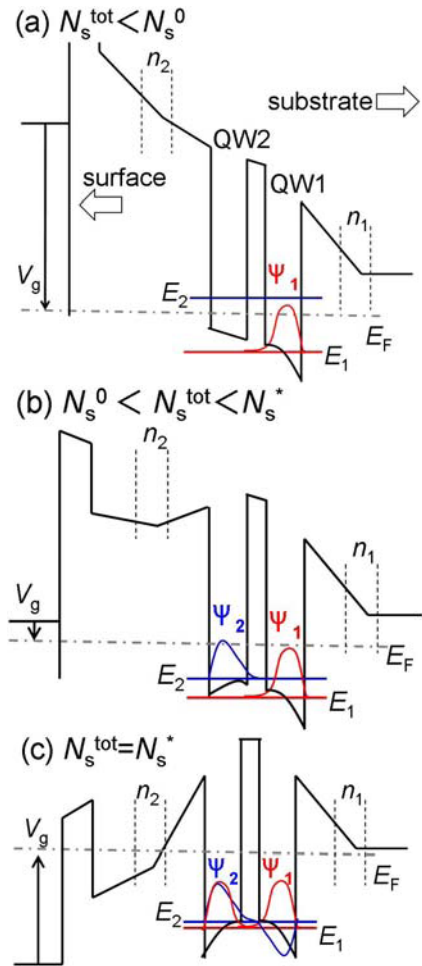
Fig. 8 Schematic potential diagrams for the double QW system for (a) $N_S^{tot} < N_S^0$, (b) $N_S^0 < N_S^{tot} < N_S^*$ and (c) $N_S^{tot} = N_S^*$.

assuming no interactions between the subbands originating from QW1 and QW2.

With this assumption, the total resistivity tensor $\overleftrightarrow{\mathbf{R}}_{tot}$ for the double QW is given as the inverse of the total conductivity tensor $\overleftrightarrow{\mathbf{G}}_{tot}$, which is in turn sum of two conductivity tensors $\overleftrightarrow{\mathbf{G}}_1$ and $\overleftrightarrow{\mathbf{G}}_2$ that are associated with QW1 and QW2, respectively. These conductivity tensor $\overleftrightarrow{\mathbf{G}}_1$ and $\overleftrightarrow{\mathbf{G}}_2$ are given as the inverse of the resistivity tensors $\overleftrightarrow{\mathbf{R}}_1$ and $\overleftrightarrow{\mathbf{R}}_2$, respectively, which can be calculated as follows.

In our previous work, we found that the SdH oscillations of single QW with single subband occupation can be well described by the following equation [1], [9].

$$\Delta R_{xx} = -4R_0 X(T) \exp\left(\frac{-\pi}{\omega_c \tau_q}\right) \cos\left(\frac{2\pi^2 \hbar N_S}{eB}\right), \quad (1)$$

where

$$X(T) = \frac{2\pi^2 k_B T/\hbar\omega_c}{\sinh(2\pi^2 k_B T/\hbar\omega_c)} \quad (2)$$

and R_0 is the resistivity of the sample at $B = 0$. We note

Table 1 Parameter values used in the simulation.

V_g [V]	N_{S2} [10^{16}m^{-2}]	N_{S1} [10^{16}m^{-2}]	τ_{q2} [10^{-14}s]	τ_{q1} [10^{-14}s]	μ [m^2/V·s]
0.4	2.2931	2.6974	15	10.5	7
0.2	2.2703	2.6809	14	10.5	7
0	2.2347	2.6711	12.7	10.5	6.5
-0.2	2.1531	2.6546	10.5	10.5	6.5
-0.4	2.0067	2.6415	8.5	10.5	6.5
-0.6	1.8658	2.6316	8	10.5	6.5
-0.8	1.6776	2.6184	7.5	10.5	6
-1.0	1.4901	2.6086	8	10	5.5

$R_0 = (eN_S\mu)^{-1}$, where μ is the electron mobility. In Eqs. (1) and (2), $\omega_c = eB/m^*$ is the cyclotron frequency, τ_q is the quantum scattering time, e is electron's charge, k_B is Boltzmann's constant, and $\hbar$ is Planck's constant divided by 2π. The effective mass value we used in our simulation is $m^*/m_e = 0.047$.

The conductivity tensor $\overleftrightarrow{\mathbf{G}}$ can be obtained by the inverse of the resistivity tensor $\overleftrightarrow{\mathbf{R}}$,

$$\overleftrightarrow{\mathbf{G}} = \begin{pmatrix} R_{xx} & -R_{xy} \\ R_{xy} & R_{xx} \end{pmatrix}^{-1} = \frac{1}{R_{xx}^2 + R_{xy}^2} \begin{pmatrix} R_{xx} & R_{xy} \\ -R_{xy} & R_{xx} \end{pmatrix}. \quad (3)$$

For QW1 and QW2, we assume $R_{xx} = (eN_S\mu)^{-1} + \Delta R_{xx}$ and $R_{xy} = B(eN_S)^{-1}$. N_S values for each QWs, denoted as N_{S1} and N_{S1}, were extracted from the experiment (Fig. 6) here. While we allowed the values of τ_qs for each QWs, denoted as τ_{q1} and τ_{q2}, respectively, to vary independently as fitting parameters, the transport mobilities μ's for QW1 and QW2 are extracted from measured resistances of the sample assuming they are equal for simplicity. All the parameter values used in our simulation, where τ_{q1} and τ_{q2} are those that fit the experimental results (Fig. 5) best, are summarized in Table 1.

5.2 Simulation Results

Shown in Fig. 9 are the R_{xx} component of the total conductivity tensor $\overleftrightarrow{\mathbf{R}}_{tot}$ as calculated above, multiplied by 2 considering the aspect ratio of the experimental Hall bar shape (length/width=2). We find that the simulated SdH oscillations are in quantitative agreement with the experimental results. Since our model does not take into account either the Rashba or Zeeman spin splitting, some of the fine features in the experimental data, such as that around $B \approx 5.2$T for the experimental $V_g = 0.4$ V curve in Fig. 5 are not reproduced well in Fig. 9. Another reason for such disagreement in the fine details is that we didn't take into account the quantization effect (quantum Hall effect) of R_{xy}.

Plotted in Fig. 10 are the amplitude of the Fourier spectrum for the simulated SdH oscillations shown in Fig. 9. We see that the change in the relative heights of the two peaks in the experimental FT spectrum as a function of V_g (Fig. 6) is reproduced in the simulated FT specrtrum. It should be noted that the peak height for QW1 increases as we decrease
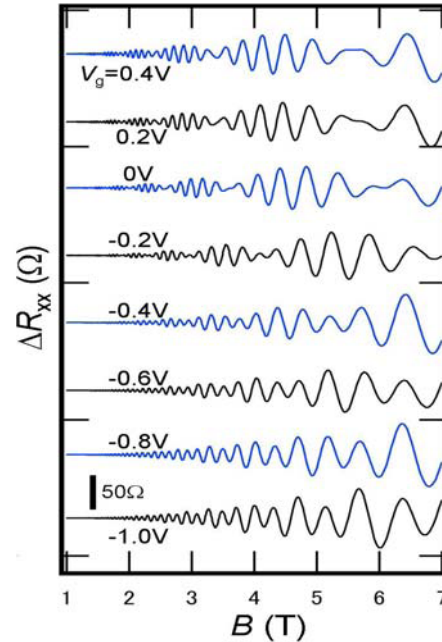
Fig. 9 Theoretically simulated results for Shubnikov-de Haas oscillations.
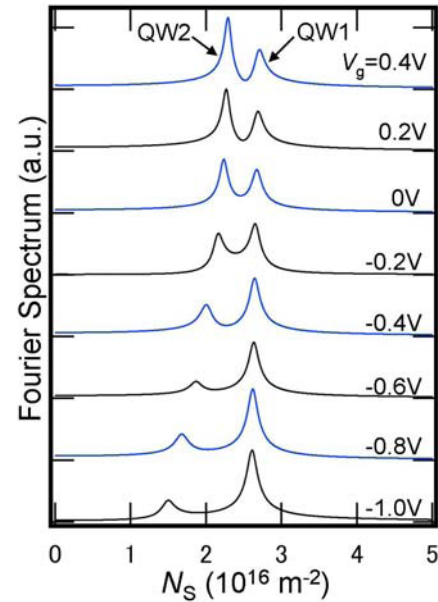
Fig. 10 Amplitude of Fourier transform spectrum for the theoretically simulated Shubnikov-de Haas oscillations shown in Fig. 9.

V_g from 0.4 V to −0.8 V, although the quantum scattering time τ_{q1} is kept constant (the electron mobility μ is slightly decreased). This means that the peak height in the FT spectrum of R_{xx} is not a direct measure of the quantum scattering time τ_q.

We finally note that we performed the Fourier transform in the simplest way without any artificial procedures such as imposing a Hann window. We nevertheless obtained well-behaved FT spectra in Figs. 6 and 10, discarding the

phase information though, since the R_{xx} values (both theoretical and experimental) decay to some constants as $1/B$ is increased, before the SdH oscillation amplitudes completely decay to zero.

6. Conclusion

We determined the value of intrinsic parameter for the Rashba effect for $In_{0.52}Al_{0.48}As/In_{0.53}Ga_{0.47}As(10\,nm)/In_{0.52}Al_{0.48}As$ (InGaAs/InAlAs) single quantum wells, lattice-matched to (001) InP substrate, from the low-temperature magneto-conductance measurements and the weak localization/antilocalization analysis. The obtained values for $a_{SO} \equiv \alpha/\langle E_z \rangle$, multiplied by the effective mass ration m^*/m_e, are $a_{SO}m^*/m_e = (1.46 - 1.51 \times 10^{-17}N_S\,[m^{-2}])$ $e\text{Å}^2$. We then designed and grew InGaAs/InAlAs double quantum wells aiming to collect basic information for realizing spin-filter devices based on the spin-orbit interaction [2]. The prepared samples were characterized by the electron transport measurements (Shubnikov-de Haas oscillations), from which electron sheet carrier densities for the lowest and second lowest subbands, denoted as N_{S1} and N_{S2}, respectively, were extracted. We have then performed theoretical simulations on the SdH oscillations for the double QW system assigning independent quantum scattering times τ_{q1} and τ_{q2} to QW1 and QW2, respectively. The quantitative agreement between the theoretical and experimental results provides useful insight toward the physics in the double QW system. Our double QWs, in combination with the built-in property of gate-controllable Rashba effect, possess a promising future for realizing novel non-magnetic spin-filter devices exploiting the matching of the spin-split Fermi surfaces between the two QWs.

Acknowledgments

References

[1] S. Faniel, T. Matsuura, S. Mineshige, Y. Sekine, and T. Koga, "Determination of spin-orbit coefficients in semiconductor quantum wells," Phys. Rev. B, vol.83, pp.115309-1–115309-7, 2011.

[2] T. Koga, J. Nitta H. Takayanagi, and S. Datta, "Spin-filter device based on the rashba effect using a nonmagnetic resonant tunneling diode," Phys. Rev. Lett., vol.88, pp.126601-1–126601-4, 2002.

[3] E.I. Rashba, Fiz. Tverd. Tela, vol.2, 1224, 1960 [Sov. Phys. Solid State, vol.2, 1109, 1960]; Y.A. Bychkov and E.I. Rashba, J. Phys. C, vol.17, p.6039, 1984.

[4] J. Nitta, T. Akazaki, H. Takayanagi, and T. Enoki, "Gate control of spin-orbit interaction in an inverted $In_{0.53}Ga_{0.47}As/In_{0.52}Al_{0.48}As$ heterostructure," Phys. Rev. Lett., vol.78, pp.1335–1338, 1997.

[5] T. Koga, J. Nitta, T. Akazaki, and H. Takayanagi, "Rashba spin-orbit coupling probed by the weak antilocalization analysis in InAlAs/InGaAs/InAlAs quantum wells as a function of quantum well asymmetry," Phys. Rev. Lett., vol.89, pp.046801-1–046801-4, 2002.

[6] G. Dresselhaus, "Spin-orbit coupling effects in zinc blende structures," Phys. Rev., vol.2, p.580, 1955.

[7] L.E. Golub, "Weak antilocalization in high-mobility two-dimensional systems," Phys. Rev. B, vol.71, pp.235310-1–235310-6, 2005.

[8] T. Matsuura, S. Faniel, N. Monta, and T. Koga, "Magnetic control of Rashba splittings in symmetric InAs quantum wells," Physica E, vol.42, pp.2707–2710, 2010.

[9] P.T. Coleridge, "Small-angle scattering in two-dimensional electron gases," Phys. Rev. B, vol.44, pp.3793–3801, 1991.

Takaaki Koga received the B.Eng. from University of Tokyo in 1992, M.S. and Ph.D. degrees in Applied Physics from Harvard University in 1995 and 2000, respectively. He is now with Division of Electronics for Informatics, Graduate School of Information Science and Technology, Hokkaido University, Sapporo, Hokkaido 060-0814. E-mail: koga@ist.hokudai.ac.jp

Toru Matsuura is now with Department of Applied Physics, Hokkaido University, Sapporo, Hokkaido 060-8628, Japan.

Sébastien Faniel received the Eng. degree in Materials Science and the Ph.D. degree in Applied Sciences from the Université catholique de Louvain (UCL) in 2000 and 2007, respectively. Until 2010, He was a postdoctoral researcher at Hokkaido University. He is now with ICTEAM Institute, UCL, Louvain-la-Neuve, Belgium. E-mail: sebastien.faniel@uclouvain.be

Satofumi Souma received B.S, M.S., and Ph.D. degree from the Department of Physics, Tokyo University of Science, Japan, in 1994, 1997, and 2000, respectively. He is now with Department of Electrical and Electronic Engineering, Kobe University, 1-1 Rokkodai Nada, Kobe, Hyogo 657-8501, Japan. Email: ssouma@harbor.kobe-u.ac.jp

Shunsuke Mineshige is now with Division for Electronics for Informatics, Graduate School of Information Science and Technology, Hokkaido University, Sapporo, Hokkaido 060-0814, Japan.

Yoshiaki Sekine received the Ph.D. degree in science from Tokyo University in 1999. He is now with NTT Basic Research Laboratories, NTT Corporation, 3-1 Morinosato-Wakamiya, Atsugi, Kanagawa 243-0198, Japan. He has worked on spintronics devices.

Hiroki Sugiyama received the B.S. and M.S. degrees in physics both from Tokyo Institute of Technology, in 1991 and 1993, respectively. He is currently a senior research engineer with NTT Photonics Laboratories, Atsugi, Japan. Since joining NTT in 1993, he has been engaged in the research and development of epitaxial growth and characterization technology of III-V compound semiconductors for ultrahighspeed electron devices. Mr. Sugiyama is a member of the Japan Society of Applied Physics and the Physical Society of Japan.